Tunable sharp and highly selective microwave-photonic band-pass filters based on stimulated Brillouin scattering

Yonatan Stern,[1] Kun Zhong,[1,2] Thomas Schneider,[3] Ru Zhang,[2] Yossef Ben-Ezra,[4] Moshe Tur,[5] and Avi Zadok[1,*]

[1]*Faculty of Engineering, Bar-Ilan University, Ramat-Gan 5290002, Israel*
[2]*Beijing University of Post and Telecommunications, Beijing 100876, China*
[3]*Institut für Hochfrequenztechnik, Hochschule für Telekommunikation, D-04277 Leipzig, Germany*
[4]*Faculty of Engineering, Holon Institute of Technology, 52 Golomb St., Holon 5810201, Israel*
[5]*School of Electrical Engineering, Faculty of Engineering, Tel-Aviv University, Tel-Aviv 6997801, Israel*
**Corresponding author: Avinoam.Zadok@biu.ac.il*

Received March 17, 2014; revised May 1, 2014; accepted May 2, 2014;
posted May 5, 2014 (Doc. ID 208420); published May 28, 2014

Stimulated Brillouin scattering (SBS) in optical fibers has long been used in frequency-selective optical signal processing, including in the realization of microwave-photonic (MWP) filters. In this work, we report a significant enhancement in the selectivity of SBS-based MWP filters. Filters having a single passband of 250 MHz–1 GHz bandwidth are demonstrated, with selectivity of up to 44 dB. The selectivity of the filters is better than that of the corresponding previous arrangements by about 15 dB. The shape factor of the filters, defined as the ratio between their –20 dB bandwidth and their –3 dB bandwidth, is between 1.35 and 1.5. The central transmission frequency, bandwidth, and spectral shape of the passband are all independently adjusted. Performance enhancement is based on two advances, compared with previous demonstrations of tunable SBS-based MWP filters: (a) the polarization attributes of SBS in standard, weakly birefringent fibers are used to discriminate between in-band and out-of-band components and (b) a sharp and uniform power spectral density of the SBS pump waves is synthesized through external modulation of an optical carrier by broadband, frequency-swept waveforms. The signal-to-noise ratio of filtered radio-frequency waveforms and the linear dynamic range of the filters are estimated analytically and quantified experimentally. Lastly, a figure of merit for the performance of the filters is proposed and discussed. The filters are applicable to radio-over-fiber transmission systems.

OCIS codes: (060.4370) Nonlinear optics, fibers; (060.5625) Radio frequency photonics; (290.5900) Scattering, stimulated Brillouin.
http://dx.doi.org/10.1364/PRJ.2.000B18

1. INTRODUCTION

Over the past three decades, microwave photonics (MWP) has been an area of much academic interest. In MWP, a radio-frequency (RF) signal modulates an optical carrier, and the modulation sidebands are processed using optical means. At the output end of the MWP system, the optical signal is detected to recover a modified RF waveform [1,2]. One important application of MWP is the transmission of RF signals over long distances using optical fibers, known as radio-over-fiber (RoF) [3–5]. RoF is used to extend the reach and coverage of wireless communication networks. The filtering of RF waveforms in the optical domain is often considered as part of RoF systems.

In the most commonly employed architecture of MWP filters [6–12], multiple RF-modulated optical signals propagate along paths of different delays and attenuation, and recombine upon detection. The realization of sharp MWP band-pass filters (BPFs) using these delay-and-sum architectures requires a large number of paths and remains challenging. In addition, the frequency response of delay-and-sum filters is inherently periodic, with multiple passbands. Filters having only a single passband would be advantageous in many RoF receivers. Other MWP filter architectures include the use of spatial light modulators [13], modulation of broadband amplified spontaneous-emission (ASE) sources in conjunction with dispersive elements [14], and more.

Alternatively, several other MWP filter realizations rely on nonlinear optical propagation effects such as stimulated Brillouin scattering (SBS). In SBS, a relatively intense pump wave amplifies a counterpropagating signal wave that is detuned in frequency by the Brillouin shift [15]. SBS amplification is simply implemented in standard fibers at room temperature, has a low power threshold of several milliwatts [15], and is highly frequency selective: its gain bandwidth is on the order of only 30 MHz [15]. SBS is therefore an attractive platform for fiber-optic sensing and signal processing applications. Examples include distributed fiber-optic sensing of temperature and strain variations [16–18], SBS-induced slow light [19], as well as tunable optical and MWP filtering [9,20–22]. SBS-based MWP BPFs are characterized by uniform transmission windows, strong out-of-band rejection, and bandwidths and central transmission frequencies that are independently reconfigurable [22]. Their frequency response is advantageously aperiodic. The selectivity of previously reported, broadened SBS-based MWP filters has been on the order of 30 dB [22].

Herein, we report a significant improvement in the performance of SBS-based MWP filters. A selectivity of up to 44 dB is experimentally demonstrated. The frequency response of the filters is very sharp: out-of-band rejection of over 30 dB is achieved within a transition bandwidth of less than 100 MHz at both edges of the passband. The shape factor of the filters, defined as the ratio of their −20 dB bandwidths and their −3 dB bandwidths, is between 1.35 and 1.5. The width of the passband is varied between 250 MHz and 1 GHz. The arbitrary and independent tuning of the central transmission frequency and of the shape of the passband is demonstrated as well.

The improvement in selectivity is obtained based on the polarization attributes of SBS in standard, weakly birefringent fibers [23,24]. One RF-modulation sideband is selectively amplified by a tailored, broadened SBS process, while an optical carrier is retained in a separate fiber path. The state of polarization (SOP) of out-of-band, unamplified spectral components within the sideband is set as orthogonal to that of the carrier; hence the reconstruction of corresponding radio frequencies upon detection is suppressed. The SOP of SBS-amplified spectral contents, on the other hand, is pulled and rotated [23,24], allowing for the recovery of corresponding radio frequencies at the detector output. SBS-based polarization pulling was previously employed in the demonstration of optical BPFs [25], in high-resolution optical spectral analysis [26–28], in the generation of advanced RF-modulation formats [29], in millimeter-wave frequency multiplication [30], in the generation of high-quality millimeter and THz waves [31], and in narrowband MWP BPFs [32].

The sharp transition between passbands and stopbands is due to the abrupt spectral edges of the SBS gain line, which are achieved in turn through the external modulation of the pump wave by linear frequency-modulated (LFM) waveforms. External modulation-based synthesis provides a simple mapping between the power spectral density (PSD) of the electrical modulating waveform and that of the generated optical sideband. LFM waveforms, in particular, are simple to generate, and their PSDs are sharp and uniform [33]. Consequently, a broadened SBS pump with a uniform PSD is obtained. External modulation by random bit sequences had been used in pump broadening for SBS-based filters [21]; however, the resulting PSD was characterized by comparatively gradual edges.

The effects of SBS pump depletion and of the ASE associated with SBS are addressed both analytically and experimentally. The power levels of both the SBS pump and signal are optimized for maximum signal-to-noise ratio (SNR) of filtered waveforms, and for maximum linear dynamic range (LDR). Practical upper bounds for selectivity, SNR and LDR are obtained. Lastly, a figure of merit for SBS-based MWP BPFs is proposed, in terms of the product of their selectivity and SNR. The upper bound on this figure of merit scales with the available pump power, and decreases with the bandwidth squared.

The remainder of the paper is organized as follows: Section 2 presents the principle of the proposed filters. The experimental setup and results are described in Section 3. Finally, a detailed discussion of the results and conclusions are provided in Sections 4 and 5. Preliminary results of this work were briefly presented in [28].

2. PRINCIPLE OF OPERATION

Figure 1 illustrates the working principle of polarization-enhanced, SBS-based MWP BPFs. An optical carrier of frequency ν_{car} is used in the generation of the SBS pump wave. The pump is modulated in a suppressed-carrier, single-sideband format, by a broadband waveform of central radio frequency f_0 and bandwidth B. Only the upper modulation sideband is retained. The sideband, which is centered at an optical frequency of $\nu_{\mathrm{car}}+f_0$, introduces an SBS amplification window of bandwidth B. The gain window is centered at an optical frequency of $\nu_{\mathrm{car}}+f_0-\nu_B$ where ν_B is the Brillouin shift in a fiber medium.

An input RF waveform is used to modulate light from the same carrier. The spectral extent of one modulation sideband is in partial overlap with the SBS amplification window (see Fig. 1). The signal and pump waves counterpropagate in a section of fiber. Those in-band spectral components of the signal sideband are amplified by SBS, and their SOP is rotated with respect to that of out-of-band components [24]. Both amplification and polarization rotation are used to discriminate between in-band and out-of-band components of the output signal. The interference of the signal sidebands and the carrier recovers a filtered RF waveform. The central transmission radio frequency of the filter is $|\nu_B-f_0|$, and its bandwidth is B (see Fig. 1).

The principle of polarization-assisted, frequency-selective SBS amplification has been detailed before [24–28], and will be repeated here only briefly. SBS gain in standard, birefringent fibers is highly polarization-dependent [23,24]. For a given SOP of the input pump, two orthogonal input signal SOPs can be identified, which provide the maximum and minimum signal power amplifications. These two states

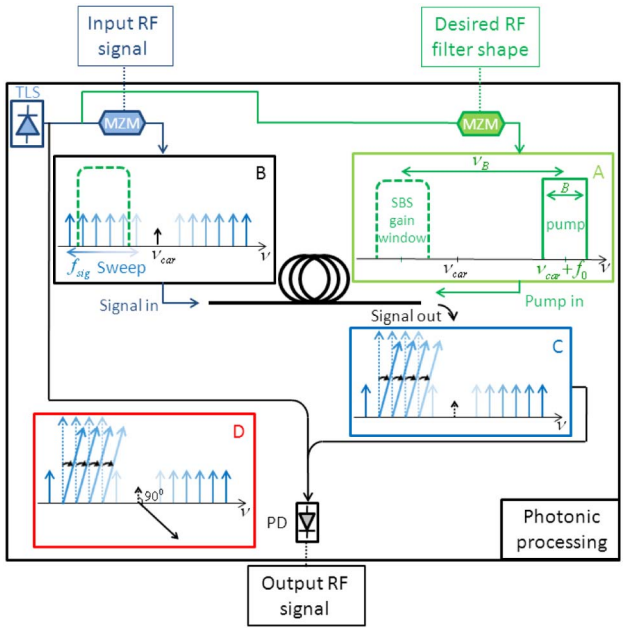

Fig. 1. Schematic illustration of the working principle of polarization-enhanced, SBS-based MWP BPFs. f_{sig}, variable radio frequency of the signal input modulation. MZM, Mach–Zehnder modulator; TLS, tunable laser source; PD, photodetector. Insets illustrate the following: A, PSD of the pump wave and the SBS gain window; B, PSD of the signal wave before the SBS amplification; C, PSD of the signal wave after the SBS amplification; D, PSD of the signal combined with the optical carrier prior to detection.

are mapped to a pair of orthogonal SOPs of the amplified signal at the output end of the fiber, whose unit Jones vectors are noted here as $\hat{e}_{\max}^{\text{out}}$ and $\hat{e}_{\min}^{\text{out}}$. For sufficiently long, randomly and weakly birefringent fibers, and in the undepleted pump regime [15], the corresponding maximum and minimum complex amplitude gain values are given by [24]

$$G_{\max}(\nu_{\text{sig}}) = \exp\left[\frac{1}{3}g(\nu_{\text{sig}})L_{\text{eff}}\right],$$
$$G_{\min}(\nu_{\text{sig}}) = \exp\left[\frac{1}{6}g(\nu_{\text{sig}})L_{\text{eff}}\right]. \quad (1)$$

Here ν_{sig} is the optical frequency of the signal, $g(\nu_{\text{sig}})$ is the complex coefficient of Brillouin amplitude gain, which is determined by the PSD of the pump wave, and L_{eff} is the effective length of the fiber. When the pump PSD is substantially broader than the inherent Brillouin gain linewidth of 30 MHz, the real part of $g(\nu_{\text{sig}})$, which governs the signal power gain, is proportional to the pump PSD with an offset of ν_B [22]. For most practical cases $G_{\max}(\nu_{\text{sig}}) \gg G_{\min}(\nu_{\text{sig}})$. Hence the SOP of the amplified signal is drawn toward that of $\hat{e}_{\max}^{\text{out}}$ [24–28].

The filtered RF waveform is reconstructed through the interference of the processed, output signal sideband with the optical carrier, of SOP $\hat{e}_{\text{car}}^{\text{out}}$. The output RF power scales with the projection of the signal output SOP onto $\hat{e}_{\text{car}}^{\text{out}}$. The carrier SOP is therefore analogous to the transmission axis of an output polarizer. Judicious alignment of $\hat{e}_{\text{car}}^{\text{out}}$ could inhibit the reconstruction of radio frequencies that correspond to unamplified optical spectral components of the signal sideband, whereas those within the SBS gain bandwidth are partially recovered. Optimal discrimination between in-band and out-of-band components is obtained when the following two conditions are met [25–28]: (a) $\hat{e}_{\text{car}}^{\text{out}}$ is aligned with equal projections on both $\hat{e}_{\max}^{\text{out}}$ and $\hat{e}_{\min}^{\text{out}}$ and (b) the SOP of out-of-band spectral components of the signal sideband, at the output end of fiber, is orthogonal to $\hat{e}_{\text{car}}^{\text{out}}$. Subject to these alignments, the RF power gain of the signal due to SBS is proportional to the following quantity:

$$|G_{\text{pol}}(\nu_{\text{sig}})|^2 = \frac{1}{4}|G_{\max}(\nu_{\text{sig}}) - G_{\min}(\nu_{\text{sig}})|^2 \xrightarrow[G_{\max}\gg 1]{} \frac{1}{4}|G_{\max}(\nu_{\text{sig}})|^2. \quad (2)$$

The in-band power gain is asymptotically 6 dB weaker than that of a corresponding so-called scalar process, in which the input signal is aligned for a maximum power gain of $|G_{\max}(\nu_{\text{sig}})|^2$. However, the rejection of the unamplified spectral components following interference with the optical carrier is theoretically infinite (since $G_{\max}(\nu_{\text{sig}}) \approx G_{\min}(\nu_{\text{sig}}) \approx 1$), whereas in the scalar processes, out-of-band components propagate through the fiber unattenuated. In the above analysis, it has been assumed that polarization mode dispersion is negligible within the spectral extent of signal and pump waves.

SBS amplification is accompanied by the generation of noise due to ASE. SBS-ASE is known to be polarized along $\hat{e}_{\max}^{\text{out}}$ [23,24]. The optical power of SBS-ASE can be estimated by

$$P_{\text{ASE}} = h\nu_{\text{car}} \cdot F_n \cdot |G_{\max}|^2 \cdot \Delta f, \quad (3)$$

where $h\nu_{\text{car}} = 1.28 \cdot 10^{-19}$ J for a wavelength of 1550 nm, F_n is the noise figure of SBS amplification (typically on the order of 150 [34]), and $\Delta f \le B$ is the measurement bandwidth of interest. In Eq. (3) it is assumed that the SBS amplification is approximately constant within Δf.

SBS-ASE degrades the SNR of filtered signals. The RF noise at the filter output is dominated by the beating between SBS-ASE and the optical carrier. Subject to the polarization alignments leading to Eq. (2), at the high-gain limit and for an undepleted pump, the ratio between the electrical power of the output signal and the electrical power of the noise photocurrent may be approximated by

$$\text{SNR} = \frac{P_{\text{sig}} \cdot |G_{\text{pol}}|^2 \cdot P_{\text{car}}}{\frac{1}{2}h\nu_{\text{car}} \cdot F_n \cdot |G_{\max}|^2 \cdot \Delta f \cdot P_{\text{car}}} \xrightarrow[G_{\max}\gg 1]{} \frac{P_{\text{sig}}}{2h\nu_{\text{car}} \cdot F_n \cdot \Delta f}. \quad (4)$$

Here, P_{sig} denotes the input optical power of the signal sideband and P_{car} denotes the optical power of the carrier at the receiver. Note the 45° angle between the SOPs of SBS-ASE and the optical carrier, which leads to the factor of 1/2 in the denominator of Eq. (4). The SNR could be improved further in the depleted pump regime [35]; however, the linearity of the filter would be compromised.

The LDR of the filter is defined as the ratio between the highest signal input power for which the filter response remains linear and the lowest input power that can be detected above the noise floor at the filter output. The LDR is restricted by SBS-ASE from below, and by pump depletion from above.

3. EXPERIMENTAL SETUP AND RESULTS

Figure 2 shows the experimental setup for the demonstration of polarization-enhanced, SBS-based MWP BPFs. The output of a tunable laser source is split into two branches using a 90/10 directional coupler. Light at the 10% arm (signal branch, blue) is modulated by a RF sine wave in double-sideband, suppressed-carrier format, and serves as a signal wave (see illustration in inset B of Fig. 1). The modulation frequency is generated by a vector network analyzer (VNA) and swept to obtain the frequency response of the filter. The output of the 90% arm is split again using a 50/50 coupler. The unmodulated optical carrier is retained in the middle branch (reconstruction branch, gray) for subsequent coherent, polarization-sensitive detection of the signal wave.

Light in the upper branch (pump branch, green) is used as a SBS pump wave. The optical spectrum of the pump is

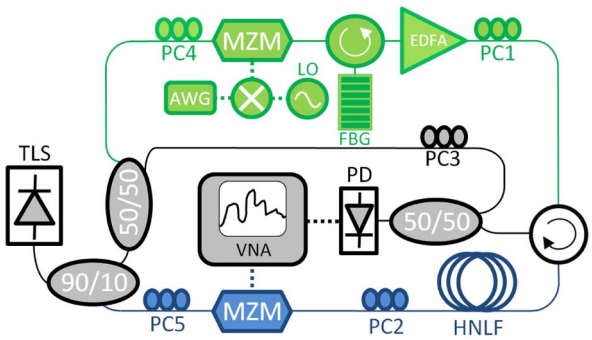

Fig. 2. Experimental setup for the demonstration of SBS-based, polarization-enhanced MWP BPFs. FBG, fiber Bragg grating.

broadened through external modulation by a RF LFM waveform, in suppressed-carrier format. LFM waveforms with a central frequency of 1 GHz and duration of 2.5 μs are generated using an arbitrary waveform generator (AWG), mixed with a RF local oscillator (LO) of frequency 6.75 GHz, and upconverted to a central frequency of $f_0 = 7.75$ GHz. The value of f_0 was chosen for convenience, due to equipment constraints. A narrowband fiber Bragg grating is used to retain only the upper modulation sideband (illustration in inset A of Fig. 1), which is then amplified using an erbium-doped fiber amplifier (EDFA) and serves as a broadened SBS pump.

The pump wave and the modulation sideband of the signal wave are launched into opposite ends of a 1-km-long highly nonlinear fiber (HNLF), with $\nu_B \sim 9.65$ GHz. The propagation time through the HNLF (5 μs) is shorter than the coherence time of the light source, but longer than the duration of the LFM waveforms used in the pump modulation. Therefore, the signal wave is subject to SBS amplification by the entire duration of the pump wave, and the pump modulation does not affect the latency of the filtering process. Following propagation in the HNLF, the modulation sidebands of the signal wave are mixed together with the optical carrier from the reconstruction branch, on a broadband photodetector (PD) (Fig. 1, insets C and D). The reconstructed RF tone is analyzed by the VNA.

The multiple polarization controllers (PCs) in the setup are aligned in accord with the considerations of the previous section. The launch SOP of the pump wave is chosen arbitrarily, and held fixed for the entire experiment. For initial calibration, the input signal wave is disconnected, and the interference between the carrier and SBS-ASE is observed. The SOP of SBS-ASE is known to be aligned with $\hat{e}_{\max}^{\text{out}}$ [23,24]. First $\hat{e}_{\text{car}}^{\text{out}}$ is aligned with $\hat{e}_{\max}^{\text{out}}$ by setting PC 3 to maximum interference of SBS-ASE and the carrier wave, and the detected RF power is noted. Next, $\hat{e}_{\text{car}}^{\text{out}}$ is readjusted through PC 3 until the power of the interference term between SBS-ASE and carrier is reduced by 50% [see the first condition in the discussion preceding Eq. (2)]. Lastly, an out-of-band signal wave is reintroduced, and PC 2 is used to adjust its input SOP until the interference between unamplified signal components and the carrier vanishes [see second condition leading to Eq. (2)].

Figure 3 shows the normalized frequency response of the MWP BPF (black solid). The measurement conditions were as follows: overall pump power of 21.3 dBm, pump bandwidth of 500 MHz, and input power of the signal modulation sideband of −32 dBm. The central frequency of the MWP BPF was $|\nu_B - f_0| = 1.9$ GHz, as expected. The full width at half-maximum of the passband was about 330 MHz, and its full width at the −30 dB points was 510 MHz. A rejection ratio of 30 dB was already reached over a transition bandwidth of less than 100 MHz on each side of the passband. The rejection ratio of out-of-band components was 44 dB, and the variations of the in-band transfer function were ±1.75 dB. The shape factor of the filter, defined as the ratio of its −20 dB bandwidth and its −3 dB bandwidth, is 1.45. The simulated filter response (red dashed) was calculated based on heterodyne measurements of the pump PSD, which determines $g(\nu_{\text{sig}})$, and using Eqs. (1) and (2). Good agreement between the shapes of simulated and experimental filters is evident. Limitations on the experimental selectivity, which do not manifest in these simulations, are addressed later.

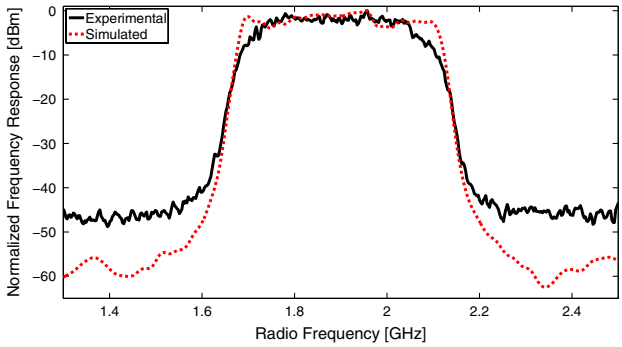

Fig. 3. Experimentally obtained frequency response of a 500-MHz-wide, polarization-enhanced, SBS-based MWP BPF (black solid) and the corresponding simulated response (red-dashed). The latter is based on measurements of the broadened pump PSD.

The central frequency of the filter could be tuned through adjustment of the LO frequency (see Fig. 2). Figure 4 shows the normalized frequency responses of MWP BPFs with central frequencies of 1.65 GHz (green), 1.9 GHz (red), and 2.15 GHz (blue). The 500 MHz tuning range of the central frequency is limited by the operational bandwidths of available RF amplifiers and filters used in the generation of LFM sequences and in driving the modulator. These limitations are not fundamental.

The bandwidth of the filter could also be tuned arbitrarily and independently by changing the sweeping range of the LFM waveform used for the pump broadening. Figure 5 shows the normalized frequency responses of MWP BPFs, obtained using pump bandwidths of 250 MHz (blue), 500 MHz (red), and 1 GHz (green). The overall pump power levels used were 18.7, 21.3, and 23 dBm, respectively. The shape factor of the filters is between 1.35 and 1.5. Finally, multiplication of the LFM waveform by an arbitrary amplitude envelope function allows for full control over the spectral shape of the filter. Three examples of MWP filters with arbitrary magnitude transfer functions are shown in Fig. 6.

Next, bounds on the selectivity, output SNR, and LDR were experimentally characterized. Although interference can provide, at least in principle, an infinite rejection of out-of-band components, the practical selectivity of the obtained MWP BPFs is limited by a residual optical carrier in

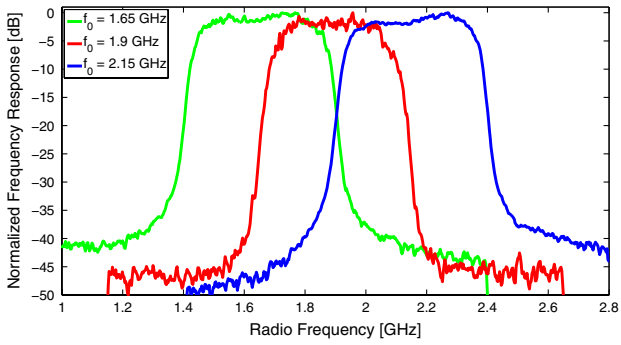

Fig. 4. Normalized frequency responses of 500-MHz-wide MWP BPFs, with central frequencies of 1.65 GHz (green), 1.9 GHz (red), and 2.15 GHz (blue).

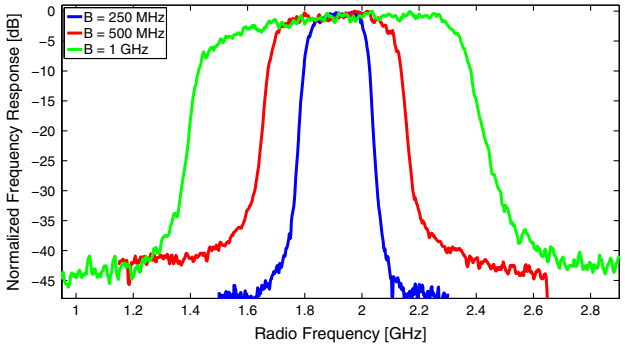

Fig. 5. Normalized frequency responses of MWP BPFs, obtained using pump bandwidths of 250 MHz (blue), 500 MHz (red), and 1 GHz (green).

the signal branch, which is not entirely suppressed by the modulator bias. The output SOP of the out-of-band, unamplified signal sideband is parallel to that of the residual carrier (Fig. 2, blue path), which leads to nonzero interference at the PD output. Figure 7 shows the selectivity of a 500-MHz-wide filter as a function of the overall input pump power. The input optical power of the signal sideband was −32 dBm. As expected, the selectivity improves with increasing pump power, until the onset of depletion at a pump power level of 20.5 dBm. The selectivity approaches an asymptotic value of 44 dB.

The SNR of the filter was quantified by measuring the output RF spectrum, with a CW input signal fixed at the center frequency of a 500-MHz-wide BPF, using different pump power levels (see Fig. 8). The input optical power of the signal sideband was optimized at each pump power level for maximum output power, below the onset of pump depletion. The amplified output tone was accompanied by a pedestal of noise due to SBS-ASE (see inset). The overall noise power was calculated by integrating the PSD of the PD output over the entire filter passband (with the signal tone excluded). The SNR initially increases with pump power as anticipated, and reaches a maximum value of 14.8 dB.

The LDR of the polarization-assisted SBS amplification process was measured by fixing a CW input signal at the central transmission frequency of the filter, and varying its input optical power level. The MWP filter was 500 MHz wide, and the pump power level was 21.3 dBm. Figure 9 shows that the output RF power scales linearly with the optical power of the input sideband tone, for input optical power levels between −59 and −31 dBm. The LDR of the filter is therefore 28 dB wide. Signals weaker than −59 dBm are lost in SBS-ASE, whereas signals stronger than −31 dBm saturate the amplification process.

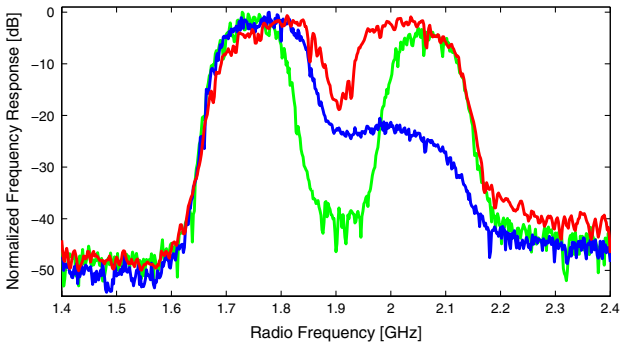

Fig. 6. Examples of normalized frequency responses of MWP filters with various magnitude transfer functions.

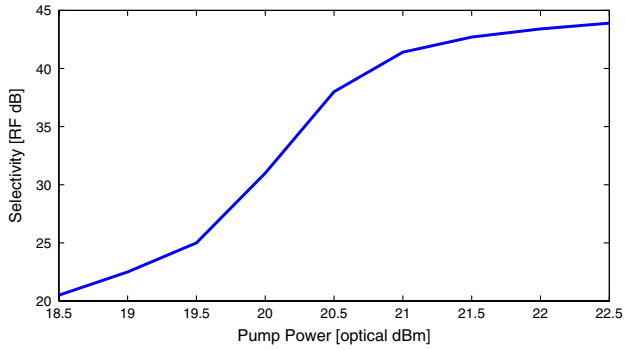

Fig. 7. Selectivity of a 500-MHz-wide MWP BPF as a function of the SBS pump power. The input optical power of the signal sideband was −32 dBm.

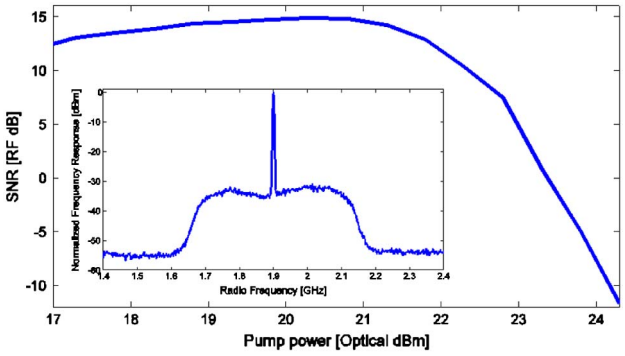

Fig. 8. SNR of a RF tone at the output of a 500-MHz-wide, MWP BPF as a function of the SBS pump power. The inset shows an example of the RF PSD at the filter output, obtained for an input CW at 1.9 GHz and pump power 20.8 dBm. A pedestal of RF noise due to SBS-ASE, spanning the entire filter passband, restricts the output SNR to 14.8 dB in this particular measurement.

4. DISCUSSION

Broadband and tunable SBS-based MWP BPFs were demonstrated, with selectivity of up to 44 dB and shape factor of 1.35–1.5. Compared with earlier corresponding demonstrations, the selectivity is improved by 10–15 dB. The selectivity

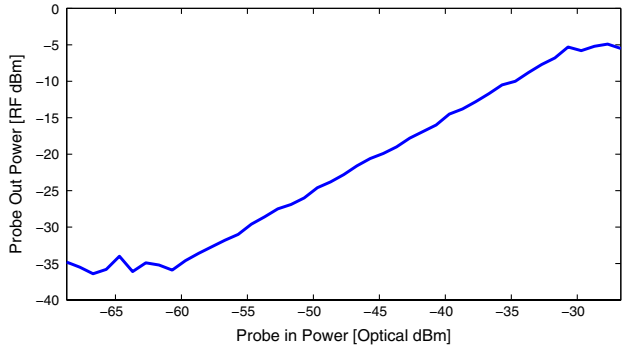

Fig. 9. LDR measurement: output electrical power of an amplified CW RF signal, as a function of the optical power of the input signal sideband.

enhancement was achieved using the polarization attributes of SBS in standard fibers. Unlike our earlier works involving SBS polarization pulling in signal processing and analysis [25–27], here the input and output waveforms were of actual radio frequencies rather than optical ones. The rejection of out-of-band components was inherently obtained through the interference of the optical carrier and sideband at the PD, which serves as an effective output polarizer.

Another advance was the synthesis of the pump PSD using external modulation by LFM waveforms. Numerous techniques for the spectral shaping of SBS pump waves appear in the literature (see a review in [19] and references therein). Examples include the use of multiple, equally spaced comb lines [36–39], and tailored direct or external modulation of a single pump carrier [21,40–42]. The bandwidth of SBS processes based on multiple comb lines is usually restricted to 200 MHz or less. Spectral broadening using external modulation is much simpler to synthesize than the direct modulation schemes we had used previously, which involved thermal and carrier-related chirp mechanisms within the pump laser diode [22,25]. External modulation using frequency-swept waveforms results in good spectral uniformity and particularly sharp edges.

The pump power that is necessary to achieve a given signal amplification factor increases with the filter bandwidth. In principle, intense pump waveforms might be distorted by Kerr nonlinearity in propagation through the HNLF. However, the pump waveforms used in our experiments consist of only a single frequency-modulated sideband without an optical carrier, and are therefore of constant magnitude, at least ideally. Hence Kerr nonlinearity is expected to introduce little distortion of the pump waves, even for relatively high power levels. No degradation in shape factor or uniformity of the filters was observed with increasing pump power levels.

The proposed filter configuration suffers from several inherent drawbacks. First, the scheme requires monitoring of environmental polarization drifts. In addition, the beating between carrier and sideband, which propagate in different physical paths, results in a reconstructed RF tone whose phase is environmentally drifting as well. These deficiencies can be alleviated with the realization of SBS-based MWP filters in integrated photonic devices on nonlinear glass, which was reported recently [43]. Next, as shown in the experiments, the SNR of filtered waveforms is limited by SBS-ASE. SNR values on the order of 15 dB were obtained for a 500-MHz-wide filter, in agreement with the prediction of Eq. (4). The obtained SNR might be inadequate for some applications, but could be well sufficient for others. For example, LFM radar waveforms at the output of SBS-based MWP BPFs were compressed with good sidelobe suppression [22]. Last, the LDR of the filter is limited by SBS-ASE from below and by pump depletion from above. Note that the measured LDR of 28 dB represents only an upper bound, as it only relates to the process of converting an optical RF-modulated sideband back to a RF waveform through SBS processing and detection. The initial electro-optic modulation, which is common to most MWP setups, is an inherently nonlinear process as well, which is susceptible to harmonic distortions and intermodulations [44]. However, modulation nonlinearities can be mitigated using elaborate modulator designs [45].

The experimentally observed LDR was narrower than expected. SBS gain saturation begins when the output optical power of an amplified signal tone of frequency ν_{sig} is about 10 dB below that of the input pump. In broadband SBS processes such as discussed here, only those spectral components of the pump wave within $\Gamma_B \sim 30$ MHz of $\nu_{\mathrm{sig}} + \nu_B$ contribute to the process. The upper limit of the experimental LDR, observed at an input signal power level of −31 dBm, agrees well with these considerations. On the other hand, the lower limit of the LDR, which is set by SBS-ASE, was higher than expected. The optical power of SBS-ASE within the measurement resolution of 3 MHz can be estimated as −70 dBm, whereas the lower limit to the LDR was met at an input signal power level of −59 dBm. Further work is needed to resolve this discrepancy.

The selectivity of the filters is limited by a residual optical carrier wave in the sideband branch of the signal wave. In the experiments, the power of the residual carrier was suppressed by a factor of $x \sim -30$ dB relative to that of the intended carrier wave. The photodetected RF power of out-of-band components scales with $4xP_{\mathrm{sig}}$, where the factor of 4 is due to the contribution of two modulation sidebands, while the RF power of in-band components scales with $(1/4)|G_{\max}|^2 P_{\mathrm{sig}}$. For a small-signal maximum SBS power gain of 30 dB, a selectivity of about 48 dB could be expected. This estimate matches well with experiments.

Finally, we note that a high power of the input signal would improve the output SNR, but on the other hand might also lead to pump depletion, and hence limited gain and selectivity. Therefore, in choosing the signal input power, a trade-off exists between selectivity and noise considerations. This trade-off can be expressed, at least roughly, in terms of a figure of merit that quantifies the quality of the filter, subject to the constraints of available pump power resources and required bandwidth. The product of SNR multiplied by the selectivity (denoted as SL) is given by

$$\mathrm{SNR} \times \mathrm{SL} \approx \frac{P_{\mathrm{sig}}}{2h\nu_{\mathrm{car}} \cdot F_n \cdot B} \times \frac{|G_{\max}|^2}{16 \cdot x}, \tag{5}$$

where large gain is assumed. This figure of merit is higher than that of a corresponding scalar SBS filtering process by a factor of $1/(32x)$, which equals approximately 15 dB in our case.

Equation (5) seems to suggest that the performance of the filter can be improved with the use of a stronger input signal. However, as mentioned above, the amplified signal power $P_{\mathrm{sig}}|G_{\max}|^2$ is restricted to a fraction $D \sim 0.1$ of the pump power that falls within the Brillouin linewidth Γ_B. We may therefore substitute

$$\begin{aligned} \mathrm{SNR} \times \mathrm{SL} &\approx \frac{1}{2h\nu \cdot F_n \cdot B} \times \frac{1}{16 \cdot x} \times D\frac{P_{\mathrm{pump}}\Gamma_B}{B} \\ &= \frac{D\Gamma_B}{32h\nu \cdot F_n \cdot x}\frac{P_{\mathrm{pump}}}{B^2} \equiv C\frac{P_{\mathrm{pump}}}{B^2}. \end{aligned} \tag{6}$$

This result indicates that the figure of merit of the filter degrades quadratically with its bandwidth, and that it is restricted by the available overall pump power P_{pump}. Given our experimental parameters, the constant C in Eq. (6) can be estimated as $5 \cdot 10^{24}$, in units of $[\mathrm{Hz}^2/\mathrm{W}]$. The SNR × SL figure of merit of a 500-MHz-wide filter, with a pump power of

21.3 dBm, for example, is expected to be 63 dB. The experimentally obtained value was 58 dB.

5. CONCLUSION

In conclusion, in this work we reported a significant enhancement in the response of MWP BPFs based on SBS, thoroughly quantified their performance, and discussed their limitations. The highly selective filters can be instrumental in all-optical signal processing within MWP systems, such as in the separation of multiple bands in ultrawideband RoF links [46].

ACKNOWLEDGMENTS

The work of Y. Stern, A. Zadok, Y. Ben-Ezra, and M. Tur was supported in part by the Chief Scientist Office, the Israeli Ministry of Industry, Trade and Labor, within "TERA SANTA" consortium. M. Tur was also supported by the Israel Science Foundation (ISF, Grant No. 1380/12). K. Zhong acknowledges the China Scholarship Council (CSC) for support of his research stay at Bar-Ilan University. The work of K. Zhong and R. Zhang was supported by the National Natural Science Foundation of China (Grant Nos. 60937003 and 61177085).

REFERENCES

1. J. Capmany, B. Ortega, and D. Pastor, "A tutorial on microwave photonic filters," J. Lightwave Technol. **24**, 201–229 (2006).
2. J. Yao, "Microwave photonics," J. Lightwave Technol. **27**, 314–335 (2009).
3. J. Capmany and D. Novak, "Microwave photonics combines two worlds," Nat. Photonics **1**, 319–330 (2007).
4. S. Pan and J. Yao, "UWB-over-fiber communications: modulation and transmission," J. Lightwave Technol. **28**, 2445–2455 (2010).
5. H. Al-Raweshidi and S. Komaki, eds., *Radio Over Fiber Technologies for Mobile Communications Networks* (Artech House, 2002).
6. D. E. Dudgeon, "Fundamentals of digital array processing," Proc. IEEE **65**, 898–904 (1977).
7. J. Capmany, B. Ortega, D. Pastor, and S. Sales, "Discrete-time optical processing of microwave signals," J. Lightwave Technol. **23**, 702–723 (2005).
8. B. Moslehi, J. W. Goodman, M. Tur, and H. J. Shaw, "Fiber-optic lattice signal processing," Proc. IEEE **72**, 909–930 (1984).
9. A. Loayssa, J. Capmany, M. Sagues, and J. Mora, "Demonstration of incoherent microwave photonic filters with all-optical complex coefficients," IEEE Photon. Technol. Lett. **18**, 1744–1746 (2006).
10. Y. Zhang and S. Pan, "A complex coefficient microwave photonic filter using a polarization-modulator-based phase shifter," IEEE Photon. Technol. Lett. **25**, 187–189 (2013).
11. A. Mokhtari, S. Preussler, K. Jamshidi, M. Akbari, and T. Schneider, "Fully-tunable microwave photonic filter with complex coefficients using delay lines based on frequency-time conversions," Opt. Express **20**, 22728–22734 (2012).
12. A. Mokhtari, K. Jamshidi, S. Preussler, A. Zadok, and T. Schneider, "Tunable microwave-photonic filter using frequency-to-time mapping-based delay lines," Opt. Express **21**, 21702–21707 (2013).
13. S. Xiao and A. M. Weiner, "Coherent photonic processing of microwave signals using spatial light modulators: programmable amplitude filters," J. Lightwave Technol. **24**, 2523–2529 (2006).
14. T. X. Huang, X. Yi, and R. A. Minasian, "Single passband microwave photonic filter using continuous-time impulse response," Opt. Express **19**, 6231–6242 (2011).
15. R. W. Boyd, *Nonlinear Optics* (Academic, 2003).
16. T. Horiguchi, T. Kurashima, and M. Tateda, "A technique to measure distributed strain in optical fibers," IEEE Photon. Technol. Lett. **2**, 352–354 (1990).
17. X. Bao and L. Chen, "Recent progress in Brillouin scattering based fiber sensors," Sensors **11**, 4152–4187 (2011).
18. M. Niklès, L. Thévenaz, and P. A. Robert, "Simple distributed fiber sensor based on Brillouin gain spectrum analysis," Opt. Lett. **21**, 758–760 (1996).
19. A. Zadok, A. Eyal, and M. Tur, "Stimulated Brillouin scattering slow light in optical fibers [Invited]," Appl. Opt. **50**, E38–E49 (2011).
20. X. S. Yao, "Brillouin selective sideband amplification of microwave photonic signals," IEEE Photon. Technol. Lett. **10**, 138–140 (1998).
21. T. Tanemura, Y. Takushima, and K. Kikuchi, "Narrowband optical filter, with a variable transmission spectrum, using stimulated Brillouin scattering in optical fiber," Opt. Lett. **27**, 1552–1554 (2002).
22. A. Zadok, A. Eyal, and M. Tur, "Gigahertz-wide optically reconfigurable filters using stimulated Brillouin scattering," J. Lightwave Technol. **25**, 2168–2174 (2007).
23. M. O. Van Deventer and A. J. Boot, "Polarization properties of stimulated Brillouin scattering in single-mode fibers," J. Lightwave Technol. **12**, 585–590 (1994).
24. A. Zadok, E. Zilka, A. Eyal, L. Thévenaz, and M. Tur, "Vector analysis of stimulated Brillouin scattering amplification in standard single-mode fibers," Opt. Express **16**, 21692–21707 (2008).
25. A. Wise, M. Tur, and A. Zadok, "Sharp tunable optical filters based on the polarization attributes of stimulated Brillouin scattering," Opt. Express **19**, 21945–21955 (2011).
26. S. Preussler, A. Zadok, A. Wiatrek, M. Tur, and T. Schneider, "Enhancement of spectral resolution and optical rejection ratio of Brillouin optical spectral analysis using polarization pulling," Opt. Express **20**, 14734–14745 (2012).
27. Y. Stern, K. Zhong, T. Schneider, Y. Ben-Ezra, R. Zhang, M. Tur, and A. Zadok, "Brillouin optical spectrum analyzer monitoring of subcarrier-multiplexed fiber-optic signals," Appl. Opt. **52**, 6179–6184 (2013).
28. Y. Stern, K. Zhong, T. Schneider, Y. Ben-Ezra, R. Zhang, M. Tur, and A. Zadok, "Frequency-selective filtering and analysis of radio-over-fiber using stimulated Brillouin scattering," in *Proceedings of the IEEE International Topical Meeting on Microwave Photonics* (2013), pp. 146–149.
29. M. Sagues and A. Loayssa, "Orthogonally polarized optical single sideband modulation for microwave photonics processing using stimulated Brillouin scattering," Opt. Express **18**, 22906–22914 (2010).
30. B. Vidal, "Photonic millimeter-wave frequency multiplication based on cascaded four-wave mixing and polarization pulling," Opt. Lett. **37**, 5055–5057 (2012).
31. S. Preussler, N. Wenzel, R. P. Braun, N. Owschimikow, C. Vogel, A. Deninger, A. Zadok, U. Woggon, and T. Schneider, "Generation of ultra-narrow, stable and tunable millimeter- and terahertz- waves with very low phase noise," Opt. Express **21**, 23950–23962 (2013).
32. W. Li, L. X. Wang, and N. H. Zhu, "All-optical microwave photonic single-passband filter based on polarization control through stimulated Brillouin scattering," IEEE Photon. J. **5**, 5501411 (2013).
33. R. J. Mailloux, *Phased Array Antenna Handbook* (Artech House, 2005).
34. R. W. Tkach, A. R. Chraplyvy, and R. M. Derosier, "Performance of WDM network based on stimulated Brillouin scattering," IEEE Photon. Technol. Lett. **1**, 111–113 (1989).
35. M. F. Ferreira, J. F. Rocha, and J. L. Pinto, "Analysis of the gain and noise characteristics of fibre Brillouin amplifiers," Opt. Quantum Electron. **26**, 35–44 (1994).
36. M. D. Stenner, M. A. Neifeld, Z. Zhu, A. M. C. Dawes, and D. J. Gauthier, "Distortion management in slow-light pulse delay," Opt. Express **13**, 9995–10002 (2005).
37. K.-Y. Song, M. González Herráez, and L. Thévenaz, "Gain-assisted pulse advancement using single and double Brillouin gain peaks in optical fibers," Opt. Express **13**, 9758–9765 (2005).
38. T. Sakamoto, T. Yamamoto, K. Shiraki, and T. Kurashima, "Low distortion slow light in flat Brillouin gain spectrum by using optical frequency comb," Opt. Express **16**, 8026–8032 (2008).
39. X. Zou, W. Li, W. Pan, L. Yan, and J. Yao, "Photonic-assisted microwave channelizer with improved channel characteristics

based on spectrum-controlled stimulated Brillouin scattering," IEEE Trans. Microwave Theor. Tech. **61**, 3470–3478 (2013).
40. A. Zadok, A. Eyal, and M. Tur, "Extended delay of broadband signals in stimulated Brillouin scattering slow light using synthesized pump chirp," Opt. Express **14**, 8498–8505 (2006).
41. A. E. Willner, B. Zhang, L. Zhang, L. S. Yan, and I. Fazal, "Optical signal processing using tunable delay elements based on slow light," IEEE J. Sel. Top. Quantum Electron. **14**, 691–705 (2008).
42. Y. Zhu, M. Lee, M. A. Neifeld, and D. J. Gauthier, "High-fidelity, broadband stimulated-Brillouin-scattering-based slow light using fast noise modulation," Opt. Express **19**, 687–697 (2011).
43. A. Byrnes, R. Pant, E. Li, D.-Y. Choi, C. G. Poulton, S. Fan, S. Madden, B. Luther-Davies, and B. J. Eggleton, "Photonic chip based tunable and reconfigurable narrowband microwave photonic filter using stimulated Brillouin scattering," Opt. Express **20**, 18836–18845 (2012).
44. L. Yaron and M. Tur, "RF nonlinearities in an analog optical link and their effect on radars carrying linear and nonlinear frequency modulated pulses," J. Lightwave Technol. **30**, 3475–3483 (2012).
45. J. H. Schaffner and W. B. Bridges, "Intermodulation distortion in high-dynamic range microwave fiber-optic links with linearized modulators," J. Lightwave Technol. **11**, 3–6 (1993).
46. M. Ran, B. I. Lembrikov, and Y. Ben-Ezra, "Ultra-wideband radio-over-optical fiber concepts, technologies and applications," IEEE Photon. J. **2**, 36–48 (2010).